Diffusion of Mesoscopic Probes in Aqueous Polymer Solutions Measured by Fluorescence Recovery after Photobleaching

Yu Cheng*,† and Robert K. Prud'homme*

Department of Chemical Engineering, Princeton University, Princeton, New Jersey 08540

James L. Thomas

Department of Chemical Engineering and Applied Chemistry, Columbia University, New York, New York 10027

Received May 4, 2001; Revised Manuscript Received July 12, 2002

ABSTRACT: Fluorescence recovery after photobleaching (FRAP) has been used to follow the diffusion of mesoscopic probes (1 nm < R < 20 nm) in aqueous poly(ethylene oxide) (PEO) and guar galactomannan solutions. We define "mesoscopic" as the regime for which the size of the diffusing species is of the same order as the screening length ξ in the polymer matrix solution. We show that diffusion depends not only on the dimensionless length scale R/ξ but also on the dimensionless time scale corresponding to the relaxation of the polymer mesh by "constraint release" vs the time for motion of the probe species over the length ξ. Two different FRAP techniques were used: fringe pattern bleaching and recovery (FPBR) and confocal scanning laser microscopy (CSLM). The effect of probe structure on diffusion through polymer matrices was investigated by measurements on probes with differing fractal dimensions (d_f): proteins and polystyrene latex particles behave as rigid spheres ($d_f = 3$); dextrans are slightly branched polymers with a more expanded conformation ($d_f = 2.3$); dendrimers fall between these two with a density first decreasing and then increasing with generation. Dendrimers at low generations (G0) and high generations (G9−G10) are compact, while the intermediate generations (G2−G6) are more porous. Probe diffusion was found to be a function of the fractal dimension of the probe: the diffusion of rigid spheres was shown to be more hindered in semidilute and concentrated polymer solutions than dextran molecules with the same hydrodynamic size in free solution. The scaling equation $D/D_0 = \exp[-\beta(R/\xi)^\delta]$ fit the experimental results well for mesoscopic, rigid spherical probes. The effects of matrix polymer stiffness and polymer molecular weight were also addressed. At constant screening length ξ (i.e., constant polymer concentration) polymers of different molecular weights are used to demonstrate the region of mesoscopic probe diffusion that is independent of the matrix polymer molecular weight. The dependence of diffusivity on the ratio of the matrix polymer persistence length l_p to the mesh size ξ was shown from measurements using the flexible PEO and more rigid guar as matrix polymers. At equal mesh size, diffusion through the more rigid matrix is hindered relative to that through the more flexible mesh; this effect becomes more pronounced as concentration increases and mesh size decreases.

1. Introduction

The diffusion of macromolecules through polymer solutions and gels is important in many industrial and biological applications. For example, a better understanding of how macromolecular drugs are transferred in living tissue is essential for the design of macromolecule-based therapies.[1,2] The transport of macromolecules across membranes, in porous chromatography supports, and in porous media is important to bioseparations.[3−5] In the food and oil industries, enzymes are often used to degrade polysaccharide chains at very high polymer concentrations.[6] The reactions are diffusion-controlled, and an understanding of the diffusion limitations is necessary to predict process performance. We have recently shown three regimes of polymer (i.e., substrate) concentration on enzymatic reaction rate for the hydrolysis of guar galactomannan by β-mannanase: (1) a low polymer concentration regime which shows zero-order kinetics with respect to polymer concentration, (2) a semidilute polymer regime which obeys Michaelis−Menten kinetics, and (3) a high concentration regime which shows diffusion limitation reaction.[7]

The motivation for the present work is to define the onset and the extent of diffusion limitation in terms of the properties of both the polymer matrix and the structure of the diffusing probe species. We will classify the extensive body of previous research on probe diffusion in polymer solutions by three parameters: (1) the size of the diffusing species (R) relative to the characteristic length for the polymer solution (ξ, the mesh size or screening length), (2) the fractal dimension of the diffusing species d_f ($d_f = 2$ for a penetrable polymer coil and $d_f = 3$ for an impenetrable sphere), and (3) the time for the matrix polymer mesh to rearrange relative to the time for the probe species to move over the length ξ. This third "dynamic" parameter is one that was first appreciated by the rheology community under the terminology of "constraint release" or "tube renewal".[8−12] The concept of constraint release appeared first in attempts to reconcile rheological data and the ideas of reptation. The concept was that, in addition to the normal mode of "test chain relaxation" by reptation along a confining tube, the "tube" itself is a dynamic entity: as other chains reptate and change the confining tube, another mode of relaxation is introduced for the test chain. In a matrix of infinitely long polymers, a

* To whom correspondence should be addressed: FAX 609-258-0211; e-mail yu_cheng@merck.com, prudhomm@princeton.edu.
† Current address: Merck Research Laboratories, WP78-304, West Point, PA 19486.

10.1021/ma0107758 CCC: $22.00
Published on Web 08/24/2002

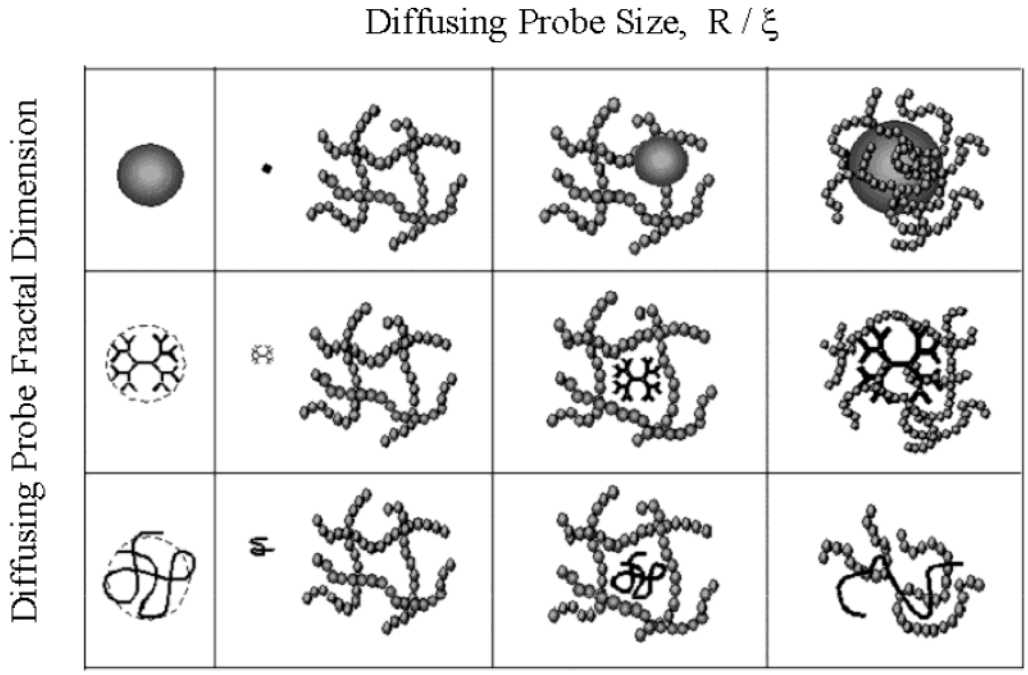

Figure 1. Diffusion of probe particles in polymeric media depends on (1) relative size scale of the diffusing species (R) to the characteristic length scale for the polymer solution (ξ, the mesh size) and (2) the fractal dimension of the diffusing species d_f ($d_f = 2$ for a penetrable polymer coil and $d_f = 3$ for an impenetrable sphere). In this study, we provide new data in the three intermediate regimes. That is, diffusion of mesoscopic sized probes (1 nm < $R \sim \xi$ < 20 nm) with fractal dimensions that span from Gaussian coils to hard spheres.

finite molecular weight test chain would relax only by its own reptation, but for test chains in lower molecular weight matrices, a substantial or even dominant amount of relaxation may arise from the motion of the matrix polymers. While the concept arose from considering polymer-in-polymer dynamics, the same concept applies to a mesoscopic probe of any fractal dimension. That is, some diffusive motion arises from temporal fluctuation of the matrix mesh with constant topology, and some motion may arise from dynamics of the matrix polymer that releases topological hindrance to motion and thus increases diffusion. It is obvious upon reflection that the process of diffusion depends not only on the average properties of the matrix through which the probe is diffusing (parameter 1: ξ/R) but also on the dynamics of rearrangement of the matrix (parameter 3). Many of the apparently contradictory conclusions in the literature come from not separating these effects. These will be discussed in more detail below. By confining most of our experiments to conditions for which the matrix mesh relaxation time is much longer than the time scale for diffusive motion of the probe, we can reduce the problem to nine diffusion regimes shown schematically in Figure 1. This experimental study provides new data in the three intermediate regimes; that is, diffusion of mesoscopic sized probes ($R \approx \xi$) with fractal dimension that span from Gaussian coils to hard spheres. In the final sections of the paper we explicitly consider the effect of mesh constraint release by studying matrix polymers over a wider range of molecular weights. We observe a regime where constraint release and mesh size both influence diffusive motion and at high enough molecular weight a regime in which diffusion depends on mesh size (ξ/R) but is independent of matrix molecular weight. This is the regime implicit in the classic scaling theory models for diffusion considered by de Gennes.[13] Finally, we study the effect of matrix polymer chain stiffness (i.e., persistence length l_p) on diffusion at constant mesh size ξ/R and show that this additional length scale l_p/ξ plays an important role, with stiffer polymers retarding diffusion relative to more flexible chains.

The diffusion of hard spheres (spherical probes) in linear polymer solutions has been extensively studied. Theoretical treatments by Langevin and Rondelez,[14] Cukier,[15] and Altenberger et al.,[16] though based on different physical models, all lead to formulas in which the reduced diffusion coefficient of the probe particle is a stretched exponential function of the concentration of the polymer matrix:

$$D/D_0 = \exp(-\alpha C^{\nu}) \tag{1}$$

where D_0 and D are diffusion coefficients of the probe in pure solvent and in polymer solution, respectively, α is a function of the probe size R, and ν is related to the solution properties of the polymer and falls between 0.5 and 1 for several systems. This phenomenological relationship was first proposed by Phillies et al.[17,18] By arguing the dominance of hydrodynamic interactions over topological effects (entanglement) in solutions, he generalized an empirical scaling equation for various tracers (hard spheres, globular proteins, linear and branched chains) in different types of polymer matrices:

$$D/D_0 = \exp(-bR^u M^x C^y) \tag{2}$$

where M is the molecular weight of the matrix polymer, $u = \pm 0.2$, $x = 0.8$, and $y = 0.5-1.0$. Similar to eq 1, eq 2 describes a stretched exponential relationship with respect to polymer concentration. However, compared to the data fit by eq 1, the reduced diffusion coefficient D/D_0 correlation of Phillies is a weaker function of the probe size R but depends strongly on the matrix polymer molecular weight. This dependence is not unexpected. However, the correlations were drawn from experi-

ments with polymer meshes that were not sufficiently entangled to eliminate constraint release as a contributing diffusion mechanism. Moreover, the latex probes used were significantly larger than the mesh size and the radius of gyration (R_g) of the matrix polymer. The conclusions of Streletzky et al.[19] included the effect of concentration changes on mesh size but do not consider the contribution of constraint release. An excellent series of studies of spherical probe mobility in polymer solutions by Tong et al.[20,21] showed that particles "feel" the single-chain viscosity rather than the solvent viscosity when their radius is much smaller than the correlation length ξ of the polymer solution. As the particle size becomes greater than the correlation length, the particle experiences the macroscopic viscosity of the polymer solution. However, they used polymers with $R_g = 8$ nm, colloid probe size of $R = 5$ nm, and concentrations that gave mesh sizes of $\xi = 3$ nm at their critical polymer concentration C_0. Increasing the polymer concentration in their experiments decreased ξ, but it also increased the amount of polymer chain entanglement and changed constraint release dynamics. In summary, these studies have not completely isolated the effects of the average static mesh size from the dynamics that affect the topological rearrangement of the mesh. Reviews of probe diffusion based on different physical models have also been presented by Masaro and Zhu[22] and Amsten.[23]

The diffusion of both small (Figure 1, $R \ll \xi$) and large probes (Figure 1, $R \gg \xi$) in polymer solutions has been extensively studied. For small probes, which are usually solvents and dye molecules, the diffusion coefficient has been shown to be independent of polymer molecular weight, despite large differences in macroscopic solution viscosities.[24] For large probes, typically large latex particles or whole cells, the diffusion coefficient is given by the Stokes−Einstein (SE) equation (eq 3):

$$D = \frac{kT}{6\pi\eta R} \tag{3}$$

where k is Boltzmann's constant, T is the temperature (K), R is the hydrodynamic radius of the spherical probe, and η is the zero-shear viscosity of the solution. This equation is based on the assumption that the medium can be treated as a continuum on the length scale of R. Positive deviations have often been reported in the dilute and semidilute concentration regimes,[25−27] possibly caused by a polymer "depletion layer" around the probe. (Dynamic light scattering, which was used for these measurements, probes mainly the small-length-scale motion of the probe particles.[21]) When the matrix concentration continues to increase to a sufficiently high value, SE behavior is recovered.[27] However, different results have been observed by Lin and Phillies: they found that the Stokes−Einstein equation fails badly for spheres in high-molecular-weight polymer solutions at high concentrations.[28]

The diffusion of probes in the transitional mesoscopic regime is less studied. This is partly due to the difficulties in finding rigid spherical probes with diameters between 1 and 20 nm, which is the convenient size range to match polymer solution mesh sizes. Globular proteins, such as lactalbumin, ovalbumin, and bovine serum albumin (BSA), have been used as hard spheres with size ranging from 2 to 10 nm. Dextrans, which are slightly branched polysaccharides, are often chosen as spherical probes in diffusion experiments, even though

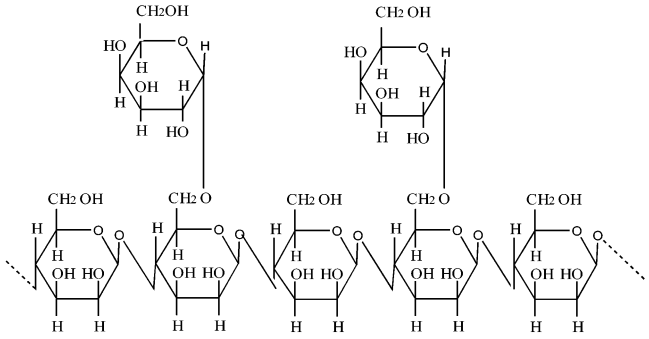

Figure 2. Structure of guar galactomannan: Guar is a natural occurring polysaccharide, consisting of a linear backbone of β-1,4-linked mannose units with α-1,6-linked galactose units randomly attached as side chains. The ratio between mannose and galactose units is about 1.7:1.

they are flexible, porous macromolecules.[29] Dendrimers are a new class of macromolecules consisting of a multifunctional core from which successive branched repeating units extend radially outward. These molecules are synthesized in a stepwise manner with new generations doubling the molecular weight, the number of end groups, and the number of branch points of the previous one. In addition, dendrimers have an extraordinarily narrow molecular weight distribution and a well-defined number of end groups. Dendrimers become increasingly spherical with successive generations, from starlike at low generation to dense sphere at higher generations.[30] Yu and Russo studied poly(amidoamine) dendrimers using both light scattering and fluorescence recovery after photobleaching (FRAP) methods. They found that fluorescently tagged dendrimers make suitable markers for probe diffusion studies.[31]

Many experimental techniques have been used to study tracer diffusion in polymer solutions and gels. Recent reviews have been presented by Muhr and Blanshard[32] and Westrin et al.[33] Dynamic light scattering (DLS) is often applied to measure the diffusion of hard spheres, usually latex particles and colloidal silica, in polymer solutions. However, strong background scattering from the matrix polymer has prevented accurate measurement of diffusion coefficient of the probe molecules in many systems. In recent years, the development of optical techniques, such as forced Rayleigh scattering (FRS)[34,35] and FRAP,[29,36−40] has provided opportunities for diffusion measurements with high sensitivity and accuracy over a very wide range.

In this study, we demonstrate the accurate measurement of self-diffusion coefficients of probes by two different FRAP experiments: fringe pattern bleaching and recovery (FPBR) and confocal scanning laser microscopy (CSLM). The diffusions of four types of probes—globular protein, polyamidoamine starburst dendrimers (PAMAM-SBDs), dextrans, and small polystyrene latexes—were measured and compared in the mesoscopic range. Two different water-soluble polymers, poly(ethylene oxide) (PEO) and guar galactomannan, were used as the matrix. Guar galactomannan is a natural occurring polysaccharide, consisting of a linear backbone of β-1,4-linked mannose units with α-1,6-linked galactose units randomly attached as side chains (Figure 2). It is widely used in a variety of industrial applications due to its low cost and ability to produce a highly viscous solution at low concentrations.[41−43]

2. Experimental Section

2.1. Materials and Sample Preparation. Four dextran fractions labeled with fluorescein isothiocyanate (FITC-dextran: 20 000 MW, 40 000 MW, 70 000 MW, and 500 000 MW) were purchased from Sigma (St. Louis, MO). Fluorescently labeled protein, ovalbumin, was obtained from Molecular Probes (Eugene, OR). Green fluorescent polymer microspheres with a diameter of 26 nm were from Duke Scientific Corp. (Palo Alto, CA).

The polymers are poly(ethylene oxide)s (PEO) with molecular weights 40 000, 200 000, and 600 000 purchased from Aldrich. To remove insoluble contaminants, the PEO samples were first dissolved in deionized water at a concentration of 1 wt % and then centrifuged at 18 000*g* for 4 h. The supernatants were removed and freeze-dried for use. The purified PEO samples were dissolved in 0.04 M phosphate buffer solution (pH = 8) at different concentrations. Fluorescent probes were added to PEO solutions at a concentration of 2 μM (with respect to fluorescein groups). The solutions were stirred slowly for 24 h before measurements.

Standard food-grade guar galactomannan was supplied by Rhone-Poulenc Inc. (Guar LJX-2), which has a molecular weight of 2×10^6 Da and $M_w/M_n \sim 2$.[7] Guar solution was prepared by adding the proper amount of polymer into 0.04 M phosphate buffer solution (pH ~8) under vigorous stirring. 0.01 wt % of sodium azide (FisherChemical) was also added as a preservative. Then the polymer solution was transferred to a container and placed on a low shear roller for approximately 20 h for complete hydration. Finally, guar solution was centrifuged in a Sovall RC5C centrifuge (DuPout) for 4 h at 17−20 °C and a speed of 16 000*g* to remove insolubles. Because of the high viscosity of guar solution, it is very hard to make solutions at concentrations >1 wt %. In addition, at high guar concentrations (>1.5 wt %), the high viscosity of the polymer solution makes (rapid) homogenization of guar and the fluorescent probe difficult. As a result, high polymer concentration samples were made by mixing guar solutions with fluorescent probes at 1 wt % and then concentrating the mixture to desired concentrations by dialysis in vacuo.

2.2. Labeling of Poly(amidoamine) (PAMAM) Dendrimers. Polyamidoamine starburst dendrimers (PAMAM-SBDs) with ethylenediamine cores of generations 6 and 8, G6 and G8, were synthesized by Michigan Molecular Institute (MMI). PAMAM-SBDs were labeled with 5-iodoacetamidofluorescein (5-IAF) dye (Molecular Probes, Inc., Eugene, OR). A protocol provided by Molecular Probes for the labeling of probes was used: Into a solution of 2 mM (in surface groups) of SBD in 20 mL of 0.01 M Na_3BO_3 (Aldrich) was added 0.05 mmol of 5-IAF in 1 mL of DMF. The reaction was run for 2 h at room temperature under stirring. The excess of free dye and salts were removed by dialysis in water using Spectra/Por cellulose ester membrane (MWCO 10 000) from Spectrum Medical Industries, Inc. The labeled probes were stored under nitrogen to avoid oxidative degradation and kept refrigerated when not used.

2.3. Diffusion Measurements and Data Analysis. a. Fringe Pattern Bleaching and Recovery (FPBR). The pattern photobleaching apparatus used has been described elsewhere.[40,44] Briefly, the 488 nm beam from a Coherent Innova 70 argon ion laser equipped with an Etalon is split with a partially silvered mirror, and the two beams are used to form an interference pattern on the sample, with a pattern spacing controlled by the crossing angle. After bleaching, an attenuated laser beam is used to illuminate the pattern, using lock-in detection: one arm of the interferometer is reflected off a piezoelectrically driven mirror, and the motion of the mirror oscillates the reading pattern over the bleached pattern. An important modification to the apparatus for this work has been the use of lock-in detection at both the fundamental frequency and at the second harmonic. When the piezo mirror is driven at the proper amplitude (spatial phase modulation of ±2.63 rad), these signals add in quadrature to indicate the pattern modulation, regardless of the spatial phase offset between the reading pattern and the bleached pattern.[45] Small temperature changes that might alter the relative path lengths of the interferometer have no effect on this quadrature signal. The decay of the signal is a simple exponential (for one component diffusion), and the diffusion constant is found as

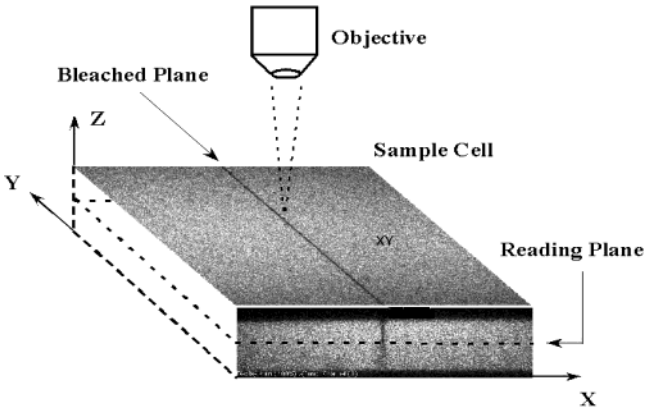

Figure 3. Bleaching profile of fluorescence recovery after photobleaching (FRAP) technique using confocal scanning laser microscope (CSLM). A thin plane is bleached with a thickness about 2 μm in a rubrene/polystyrene sample at room temperature, where the dye is essentially immobile. The sample thickness (z direction) is approximately 200 μm. The low divergence of the laser from the 20× objective used ensures a thin bleached plane through the sample.

$$D = \frac{1}{\tau q^2} \tag{4}$$

where τ is the time constant and

$$q = \frac{2\pi}{d} = 4\pi \sin \theta/\lambda \tag{5}$$

is the wavenumber of the bleached pattern. The pattern periodicity is d, the half-crossing angle of the beams is θ, and λ is the wavelength of light.

b. Confocal Scanning Laser Microscopy (CSLM). Measurements of diffusion were also made using an Olympus Fluoview confocal scanning laser microscope (CSLM) using the standard 5 mW air-cooled argon ion laser at 488 nm. A UplanFl 20×/0.50 N.A. infinity corrected objective (Olympus) was used. Samples were loaded between a microscope slide and a coverslip. A plastic spacer was used to keep a constant perpendicular spacing of approximately 200 μm. Samples were first positioned so that the focal plane was at least 50 μm away from either the coverslip or slide surface. For bleaching, full laser intensity was scanned repeatedly in a line for typically 1−4 s. In a separate experiment using rubrene dye immobilized in a polystyrene film, we determined that scanning the beam in a line with this low numerical aperture objective produces a nearly planar bleach (Figure 3). Consequently, the diffusive recovery problem is essentially one-dimensional. After bleaching, a series of images of the sample are taken (256 × 256 pixels, 2.76 μm/pixel) with the laser attenuated with neutral density filters to 6% full intensity. Depending on the diffusion coefficient of the probe, the frame rate ranges from 2.3 to 16 s/frame. The images are analyzed using MATLAB software, as follows: first, an average profile through the bleached line is computed for each image. Second, each profile is fit to a Gaussian shape (Figure 4), with the depth, width (σ), and plateau as free parameters. For simple, one-component diffusion, the transient concentration profiles have been solved as[46]

$$C(x,t) = \frac{M}{2\sqrt{\pi Dt}} \exp(-x^2/4Dt) \tag{6}$$

where D is the diffusion coefficient and M is the integrated excess (or deficit) concentration. The squared width of the

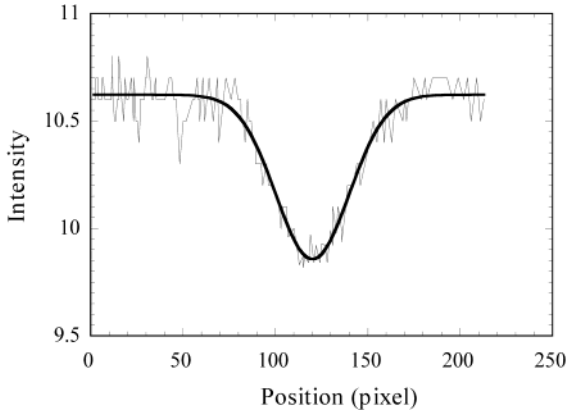

Figure 4. FRAP images are analyzed using a MATLAB software: the bleaching profile is integrated through the bleaching line and then fit to a Gaussian shape, with the depth, width, and plateau height as free parameters. The Gaussian profile broadens with time during the recovery.

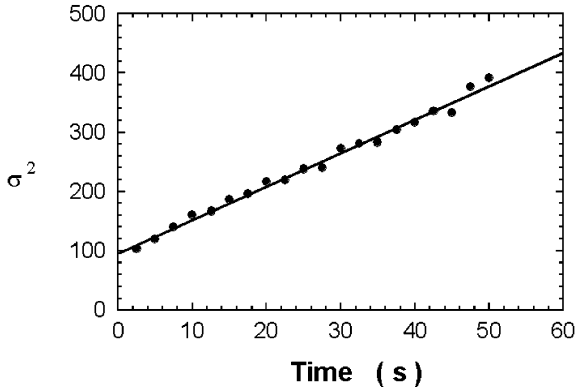

Figure 5. Standard deviation (squared width) of the Guassian profile is plotted as a function of recovery time, according to eq 6. The data fit to a straight line, and the diffusion coefficient can be obtained from the slope.

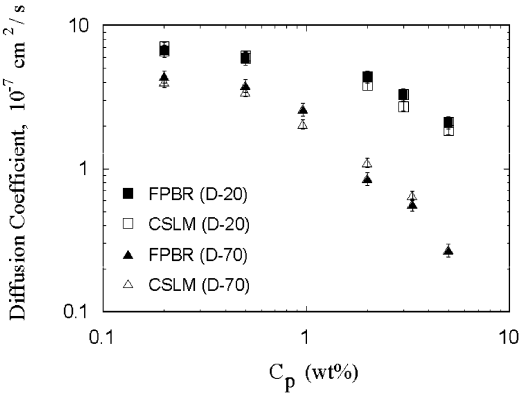

Figure 6. Two FRAP setups, Fringe pattern bleaching and recovery (FPBR), and confocal scanning laser microscopy (CSLM) were compared by studying the diffusion of dextrans (MW = 20 000 and 70 000) in guar solutions at different concentrations. Consistent diffusion results were obtained.

profile will increase in proportion to time, with a slope of 2*D*. The data fit a straight line (Figure 5).

3. Results and Discussion

3.1. Diffusion Measurements. The self-diffusion coefficient of dextrans, MW = 70 000 (D-70) and MW = 20 000 (D-20), in guar solutions were measured using both FPBR and CSLM. Figure 6 is a double-logarithmic plot of the diffusion coefficients as a function of polymer concentrations by the two techniques. For both D-70 and D-20, the probe diffusion coefficient decreases with increasing guar concentration. At low guar concentrations (c_p < 1 wt %), the diffusion coefficient asymptotically approaches the value in pure solvent, whereas at higher concentrations (c_p > 1 wt %), the diffusivity decreases markedly. Over a wide range of matrix polymer concentrations, FPBR and CSLM gave similar results within experimental error. In the absence of guar, the diffusion coefficients are 4.18×10^{-7} cm^2/s for D-70 and 7.5×10^{-7} cm^2/s for D-20. The hydrodynamic radii can be estimated using eq 3 to be 5.72 and 3.19 nm, respectively, in agreement with values previously reported by Lebrun and Junter[3] and Pluen et al.[38] The diffusion coefficient vs matrix concentration was fit to a stretched exponential (eq 1). The fitting parameters will be discussed below.

The two FRAP techniques yield consistent results, but each is more convenient for a different range of diffusivities. For the FPBR, fringe patterns are created by crossed lasers. Fringes with width between 0.5 and 100 μm can be accessed by changing the angle of intersection. This gives a broad measurable range for diffusion coefficients. By adjusting the fringes, FPBR can measure diffusion coefficients down to 10^{-16} cm^2/s in a reasonable experimental time scale. However, this technique is not accurate for measuring fast diffusion ($D \geq 10^{-6}$ cm^2/s) where the relaxation time is comparable to the bleaching time. (In principle, this limitation could be overcome with a more powerful laser.) By contrast, the confocal microscope delivers all laser power to a narrow plane in the sample, so bleaching is faster. Moreover, there is no characteristic length scale for the CLSM method. By monitoring a series of Gaussian curves over time, CSLM can cover a wide range of diffusion coefficients. Theoretically, CSLM can measure very slow diffusion. But experimentally, the measurement might take too long (hours) for $D < 10^{-10}$ cm^2/s. Hence, by CSLM, a good range of diffusion coefficient measurement is from 10^{-5} to 10^{-10} cm^2/s, which is ideal for studying the diffusion of mesoscopic probes.

The measurement of probe diffusion is often complicated by different factors, such as specific probe−polymer interactions and polymer-induced probe aggregation. One important advantage of using FRAP experiment is the high sensitivity of fluorescence signals. This allows us to use extremely low probe concentrations ($\sim 10^{-6}$ M) to minimize phase separation and probe aggregation. For ovalbumin, 0.04 M phosphate buffer was used to control the solution pH $\sim$ 8, far above the isoelectric point of ovalbumin, 4.8. Diffusion measurements were conducted at several different ionic strengths in the range of 0.01−0.08 M phosphate, and no significant differences were observed. For dendrimers, solution pH is adjusted to pH 4 to ionize the surface amine groups and minimize the possible aggregation of probes. An advantage of the CSLM technique is that we can look at the homogeneity of the sample by using the microscope. In addition, with CSLM, the presence of a nondiffusing fraction can be readily observed by a persistent "spike" at the bottom of the profiles. In this study, most experiments were done by the CSLM unless otherwise mentioned.

3.2. Fractal Dimensions. Macromolecules in solution can be described in terms of their fractal dimension d_f, defined by the scaling law[47]

$$M \propto r^{d_f} \quad (7)$$

where M and r are their mass and size, respectively. For a rigid sphere, $d_f = 3.0$. $d_f = 2$ for a linear Gaussian polymer coil (random walk) at θ conditions, and $d_f < 2$ for polymers with excluded-volume interactions.

Figure 7 shows a double-logarithmic plot of the probe molecular weight vs size, where size is the hydrodynamic radius measured by CSLM and calculated according to eq 3. The "size" r in eq 7 is the "mass radius" whereas the experimentally measured quantity in the diffusion measurement is the "hydrodynamic radius". These two lengths are proportional to each other, but the proportionality coefficient varies slightly depending on the fractal dimension of the object and hydrodynamic screening. The probes are polystyrene latex (PSL) particles, globular proteins (lactalbumin, ovalbumin, and BSA), dendrimers (G0−G10) and dextrans (D-20, D-40, D-70, D-500) in deionized water. Figure 7 also includes the size data for dendrimers provided by MMI, which were measured by viscometry and transmission electron microscopy. The three protein molecules and the PSL particle fall almost on the same line with a slope $d_f \approx 3.1$. Since the densities of PSL particle ($\rho \sim 1.04$ g/mL) and globular proteins ($\rho \sim 1-1.1$ g/mL[48]) are similar, this slope indicates a rigid spherical conformation in solution. [The typical density value for dry proteins (ρ_0) is approximately 1.3 g/cm^3. The ratio f/f_{min} for globular proteins in aqueous solution is about 1.25, in which f and f_{min} are the friction coefficient of a protein molecule and a hard sphere, respectively. Therefore, the density of a globular protein molecule in solution can be estimated by $\rho = \rho_0(f_{min}/f) \sim 1.05$ g/cm^3.] We treat globular proteins as rigid colloidal particles because their conformations are restricted on the mesoscopic length scale due to strong intramolecular attractions (hydrophobic interactions, hydrogen bonding, and van der Waals forces). The fractal dimension of dextrans $d_f \approx 2.3$ is in agreement with previously published results by Smit et al.[49] and Bu and Russo.[29] That $d_f > 2$ is thought to arise from partial branching of dextran. However, at the same molecular weight, dextrans have a much larger diameter than protein molecules, and the difference increases as molecular weight increases. At MW = 70 000, the dextran molecule is almost twice as big as the globular protein because the dextran is not a hard-sphere probe particle. The molecular weight vs size plot for dendrimers cannot be fitted to a straight line. Since the effective fractal dimension of dendrimer increases with generation, dendrimers are more densely packed at higher generations. The structure of dendrimer represents a part of an infinite network of a type known as the Bethe lattice (an infinite, regular Cayley tree).[50] Our dendrimers comprise Cayley trees with a coordination number $z = 3$, which means each junction point has z nearest neighbors. As the structure grows in space, the density of the molecule increases theoretically without limit. The last three generations, G8−G10, can be fitted to a straight line with a slope about 4.1. The mass of the dendrimer increases as the fourth power of the diameter, faster than the increase of volume (cube as diameter). This crowding problem prevents the synthesis of fully substituted dendrimers of generation higher than G10.

It is interesting that dendrimers at high molecular weight (G9 and G10) fall on the same line as the rigid particles, whereas in the intermediate molecular weight region, they have a more expanded conformation. As the dendrimers grow, they become starlike with internal porosity and structural flexibility, like the dextrans. However, with the increase of generations the dendrimer (G8−G10) becomes more densely packed due to chain crowding, and the structure approaches the density and impenetrability of a solid latex sphere or globular proteins. Models of PAMAM dendrimer structure also show that the density decreases up to generation 6 and then increases.[51,52]

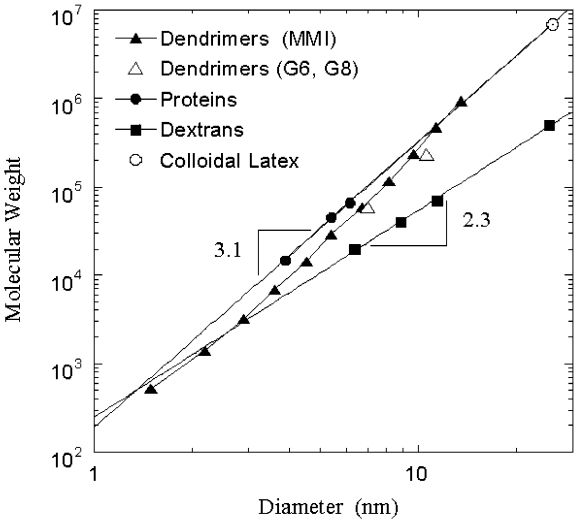

Figure 7. Probe molecular weight as a function of its hydrodynamic size in aqueous solution for dendrimers, proteins, dextrans, and polystyrene latex (PSL) particles. The three protein molecules (lactalbumin, ovalbumin, and bovine serum albumin) and the PSL particle fall on the same line with a slope $d_f \sim 3.1$, indicating a rigid spherical conformation in solution. The fractal dimension of dextrans is about 2.3, suggesting dextran is not a rigid probe particle. The effective fractal dimension of dendrimer increases with generation (strictly speaking, dendrimers are not fractals). Dendrimers at low MW (G0) and high MW (G9 and G10) all fall on the same line as the rigid particles, whereas in the intermediate molecular weight region they have a more expanded conformation.

3.3. Effect of Fractal Dimension on Hindered Diffusion. Since we have shown that rigid spherical probes have fractal dimensions different from those of the slightly branched polymeric probe dextrans, we use these probes to explore how differently the probes "see" the concentrated polymer mesh. The lower fractal dimension dextran is more able to interpenetrate the matrix polymer mesh than are the compact probes. As the polymer mesh size decreases to that of the diffusing probe species, the probe diffusion becomes hindered. The diffusion of the compact and relatively impenetrable G8 dendrimer and ovalbumin ($d_f \approx 3$) is compared to that of the more open D-20 and D-70 dextran polymer ($d_f \approx 2.3$) as they diffuse through a continuous matrix of PEO (poly(ethylene oxide)). The two sets comprise a low and high fractal dimension probe with nearly the same diffusion coefficient in pure solvent (Table 1) and allow a comparison of the importance of fractal dimension on diffusion. The data for both sets are shown in Figures 8 and 9. PEO of $M_w = 40\,000$ was used as the matrix for ovalbumin and D-20 probes and $M_w = 200\,000$ for the larger dendrimer and D-70 probes. The overlap concentration c^* of the polymer solution is also shown in the figures.

At concentrations below c^* of the PEO, the diffusion coefficient decreases with increasing matrix concentra-

Table 1. Diffusion Coefficients in Free Solution (D_0), Hydrodynamic Radii (R_h), and Stretched Exponential Fitting Parameters According to Eq 1, $D \sim D_0 \exp(-\alpha c^{\nu})$, for Different Probe Particles

	D_0, 10^{-7} cm^2/s	R_h, nm	α	ν
D-20	7.6	3.15	0.15 ± 0.02	0.66 ± 0.04
ovalbumin	8.8	2.71	0.12 ± 0.02	0.79 ± 0.05
D-70	4.18	5.72	0.19 ± 0.01	0.82 ± 0.04
G-8	4.37	5.47	0.28 ± 0.01	0.97 ± 0.03

tion in both figures. The diffusion coefficient of D-20 decreases more rapidly than that of ovalbumin (Figure 8). In this dilute range, polymer chains are individually dissolved coils and can be treated as "particles" through which the probe particle diffuses. The probe−polymer interactions can be characterized by a cross virial coefficient A_{12} with 1 standing for PEO and 2 standing for dextran or ovalbumin. The interaction is repulsive when $A_{12} > 0$ and attractive when $A_{12} < 0$. It has been shown that PEO/dextran has a higher cross virial coefficient than PEO/ovalbumin (about 2×10^{-3} mL mol/g^2 for PEO/dextran and 0.6×10^{-3} mL mol/g^2 for PEO/ovalbumin).[53−55] This indicates that the PEO/dextran interaction is more repulsive than is PEO/ovalbumin. As a result, the stronger repulsive interaction between PEO and dextran results in a slower diffusion coefficient for dextran. Another reason for the more rapid decrease of the dextran may be due to entanglement couplings that can occur during molecular collisions between the linear dextran and PEO chains.

Above c^* for the matrix the trends reverse, and dextran diffuses more rapidly than the compact probe. The greater conformational flexibility of dextran facilitates its motion through the crowded PEO matrix. The reduced diffusion coefficient D/D_0 vs polymer concentration was fit to the stretched exponential function (eq 1), and the fitting parameters are listed in Table 1. The diffusion of both the spherical probes and the dextrans fit well to a stretched exponential. Spherical probes gave higher stretched exponential powers than did the dextrans.

The two experiments show that rigid spheres ($d_f \approx 3$) are more hindered in semidilute or concentrated polymer solutions than the loosely branched polymer probes ($d_f \approx 2.3$). The difference in diffusion coefficient is more pronounced at higher probe molecular weight. In concentrated polymer solutions, probes are trapped in a polymer mesh with a characteristic mesh size. Diffusion requires either that the mesh size fluctuates or that the probe itself fluctuates and can therefore penetrate through the small mesh. Spherical probes are rigid and cannot change in size, whereas the flexibility of dextrans hastens interdiffusion. To pass through the polymer mesh, dextran coils can stretch to an ellipsoidal conformation, so that the cross section becomes small compared to a relaxed spherical polymer coil. The conformational flexibility permits dextrans, with their lower fractal dimension, to diffuse faster than rigid spheres in polymer solutions. This proposed motion can be thought of as the onset of reptation behavior.

3.4. Diffusion Models for Rigid Spherical Probes in the Mesoscopic Regime. Various models have been proposed to describe the diffusion of rigid spherical probes in polymer solutions and gels. In semidilute polymer solutions, de Gennes[13] and co-workers[14] have argued for the existence of a scaling law:

$$f_0/f_c = \psi(R/\xi) \tag{8}$$

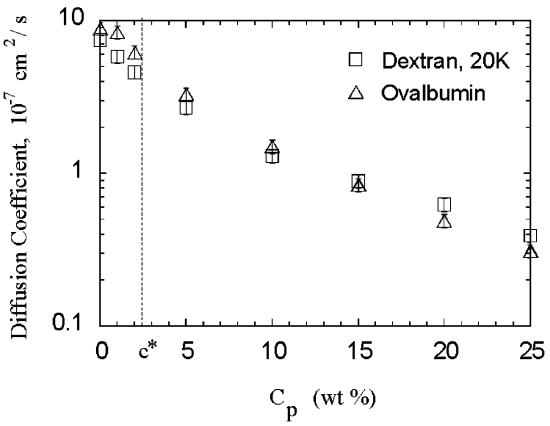

Figure 8. Diffusion coefficient of ovalbumin and dextran MW = 20 000 (D-20) in PEO solutions as a function of matrix concentration. Each data point is the average of eight different measurements. At high polymer concentration, the diffusion of ovalbumin is more hindered in the polymer matrix than D-20.

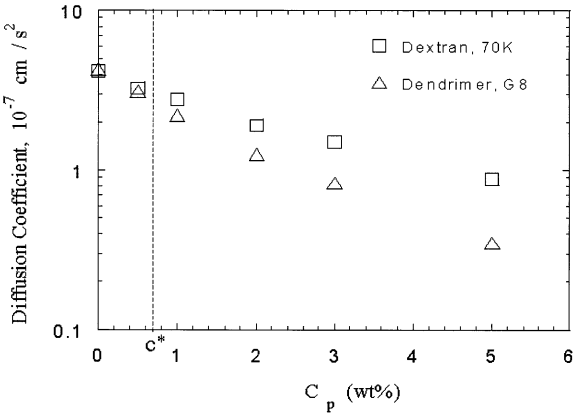

Figure 9. Diffusion coefficient of dendrimer G8 and dextran MW = 70 000 (D-70) in PEO solutions as a function of matrix concentration. The diffusion coefficient of G8 drops much faster with polymer concentration compared to D-70.

where f_0 and f_c are the friction coefficient at zero concentration and concentration c, respectively, R is the radius of the particle, and ξ is the correlation length of the polymer solution. They argued that $\psi(R/\xi) \sim 1$ for $R/\xi \ll 1$ and $\psi(R/\xi) \sim \eta_0/\eta_M$ for $R/\xi \gg 1$, where η_0 is the viscosity of the solvent and η_M is the macroscopic viscosity of the solution. More recently, Tong and coworkers found that the particles "feel" the single-chain viscosity rather than the solvent viscosity when their radius is smaller than the correlation length ξ.[20] In addition, the transport of probe particles through the transient polymer network can be considered as a process where the probe particle passes through the polymer mesh. In the mesoscopic regime where R is of the same order of ξ, the diffusion will be dominated by the fluctuations of the mesh size, and an activation energy term can be introduced by a scaling analysis to be proportional to $(R/\xi)^{\delta}$. Therefore, the reduced diffusion coefficient can be written as

$$D/D_0 = \exp[-\beta(R/\xi)^{\delta}] \tag{9}$$

The correlation length ξ can be estimated by[13]

$$\xi \approx R_g(c^*/c)^{\gamma} \tag{10}$$

where R_g is the radius of gyration of the polymer, c^* is

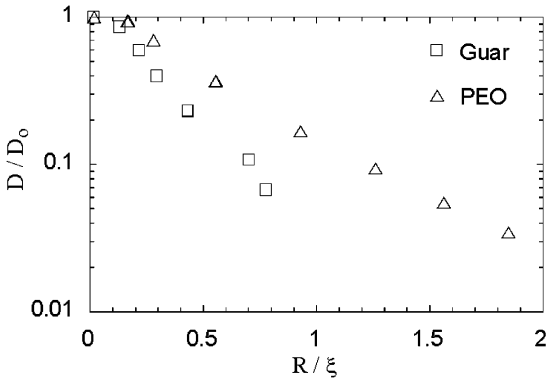

Figure 10. Effect of the matrix polymer: the reduced diffusion coefficient (D/D_0) of ovalbumin is plotted as a function of the ratio of probe radius to the polymer mesh size (R/ξ) in both guar and PEO aqueous solutions.

the overlap concentration, and γ is the scaling coefficient defined below. Hence, eq 9 can be rewritten as a stretched exponential function of polymer concentration

$$D/D_0 = \exp(-\alpha c^{\gamma\delta}) \tag{11}$$

in which $\alpha \propto R^{\delta}$. Several theories predicted that $\delta = 1$,[15,16,56] so that eq 11 becomes the same as eq 1. If we assume $\delta = 1$, from polymer scaling theory,[13]

$$R_g \sim N^u \tag{12}$$

$$\gamma = -u/(1 - 3u) \tag{13}$$

where N is the degree of polymerization and u is the dependence of R_g on the molecular weight of the polymer. For flexible polymers, u is equal to 0.5 in θ solvent and 0.6 in good solvent. According to eq 13, $\gamma = 0.75$ for good solvent and 1 for θ solvent. Therefore, the stretched exponential power is related to the solution properties of the matrix polymer.

a. Effect of Matrix Polymers. There are several effects of matrix polymers on the probe diffusion coefficients: First, the solvent quality for the polymer has an influence on the stretched exponential power ν, as discussed above. Second, the fluctuation of the polymer mesh affects the diffusion of probes. Flexible polymer chains undergo fluctuations in mesh size with greater amplitudes, whereas rigid rods should have smaller fluctuations because of their greater persistence length. The concept of stiffer and more sterically hindered chains having smaller fluctuations is the basis for the successful theory of solute diffusion through bulk polymer phases of Duda and Vrentas.[57] Decreasing of fluctuations leads to increasing the activation energy for the diffusion of a probe. Figure 10 compares the reduced diffusion coefficient D/D_0 of ovalbumin in guar and PEO aqueous solutions as a function of the ratio R/ξ. The PEO is flexible with a persistence length of about 8 Å,[58,59] and guar is stiffer with a persistence length about 40 Å.[60,61] Since water is a good solvent for both PEO and guar, we calculated the polymer correlation length $\xi \approx R_g(c/c^*)^{-0.75}$ at concentration c. Here the overlap concentration $c^* \approx 1/[\eta]$, in which $[\eta]$ is the intrinsic viscosity of the polymer. $[\eta]$ is related to the polymer molecular weight by the Mark−Houwink−Sakurada (MHS) relationship

$$[\eta] = KM_w^{\ a} \tag{14}$$

where K and a are constants. The MHS relationships for guar and PEO in aqueous solution are $[\eta] = 3.8 \times 10^{-4}M_w^{0.723}$ dL/g (guar)[62] and $[\eta] = 1.25 \times 10^{-4}M_w^{0.78}$ (PEO).[63] The radius of gyration of native guar and PEO (MW = 200 000) is 150 and 24 nm, respectively.[64,65] In Figure 10, the diffusion of ovalbumin is much slower in guar than in PEO at the same R/ξ, and the difference increases with polymer concentration. At $R/\xi \sim 0.6$, the reduced diffusion coefficient in guar is only about half of that in PEO. This is confirmation of the role of polymer backbone stiffness, at constant mesh correlation size, on diffusion of compact probes.

b. Effect of Polymer Molecular Weight. The scaling theory of de Gennes predicts that the reduced diffusion coefficient is independent of polymer molecular weight (MW) whenever $c > c^*$, because the mesh size is a function of only the polymer concentration in the semidilute and concentrated regimes.[13] For mesoscopic probes, the reduced diffusion coefficient should be independent of matrix MW as long as the polymer mesh persists for a long time, compared to the time required for the probe to "hop" a distance equal to the correlation length. However, even in the semidilute regime the polymer matrix can relax by constraint release[8,9−12]. Therefore, if the characteristic time for diffusion and tube renewal are τ_d and τ_r, when $\tau_d \ll \tau_r$, the polymer network can be treated as quasi-static. When $\tau_d > \tau_r$, the diffusion will be dominated by relaxation of the network instead of the hopping mechanism of probes. The diffusion time, τ_d, can be estimated by ξ^2/D. The relaxation time τ_r is estimated by[66]

$$\tau_r = \frac{1+k}{k}\frac{\eta_0}{G_N^0} \tag{15}$$

where $\eta_0(c_p,M)$ and $G_N^0(c_p)$ are the viscosity and the plateau modulus of the solutions, respectively. (The viscosity is a function of polymer concentration and molecular weight, and in the semidilute solution the plateau modulus is a function of polymer concentration alone.) The parameter k is a constant, which experimentally has been shown to have a value of 0.56. The plateau modulus of PEO solution was calculated using[67]

$$G_N^0 = \phi^2 G_N^0(\text{bulk}) \tag{16}$$

where G_N^0(bulk) is the plateau modulus for PEO melt and ϕ is the volume fraction of polymer in the solution. The G_N^0(bulk) value for PEO was reported by Wu to be 1.8 MPa.[68] At 5 wt % PEO (MW = 200 000) solution, $(G_N^0)_{soln} \sim 4 \times 10^3$ Pa, $\eta \sim 0.03$ Pa·s, and $\xi \sim 4.8$ nm. Assuming the probe diffusion coefficient to be 10^{-7} cm^2/s, the diffusion time is approximately 2×10^{-6} s. τ_r is calculated to be 2×10^{-5} s according to eq 16. Therefore, $\tau_d < \tau_r$, and the mesh is quasi-static on the time scale of the diffusion.

Figure 11 shows the measured diffusion coefficient of ovalbumin in PEO solutions as a function of polymer MW as well as concentration. All experiments were performed in the semidilute regime; i.e., the concentration of PEO is above the overlap concentration. We can see that at low PEO concentration (2 wt %), the diffusion coefficient decreases with polymer MW, due to the relaxation of the polymer mesh. At higher polymer concentrations (>5 wt %), the diffusion coefficient

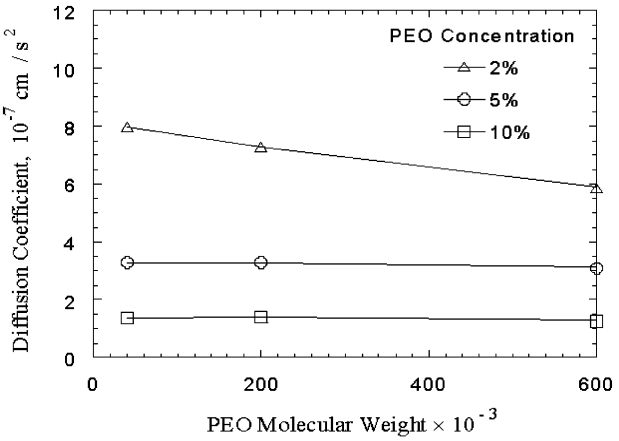

Figure 11. Diffusion coefficient of ovalbumin in PEO solutions as a function of polymer MW and concentration.

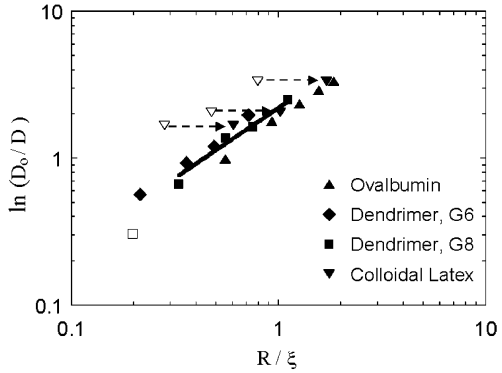

Figure 12. Reduced probe diffusion coefficient vs the ratio of probe radius to mesh size (R/ξ) for different probes: ovalbumin, dendrimers (G6 and G8), and PSL particle. A master curve is obtained based on the scaling law (eq 9), and fitting of the data yields $d = 0.95$ and $b = 2.2$.

becomes independent of the MW of the matrix polymer, and diffusion is dominated by the hopping of the probe molecule.

c. Master Plot for Compact Probes. According to eq 9, we plot $-\ln(D/D_0)$ as a function of R/ξ for different spherical probes in PEO solution (MW 200K and 600K) (Figure 12). From ovalbumin ($R \sim 2.7$ nm), G6 ($R \sim 3.6$ nm), to G8 ($R \sim 5.4$ nm), all diffusivities fall on the same master curve, supporting the scaling law (eq 9) for mesoscopic rigid probes. The diffusion of a spherical latex particle ($R \sim 13$ nm, ▽ in Figure 12) is slower compared to other probes because the PEO matrix polymers are known to absorb onto the latex sphere.[69] The increase in hydrodynamic radius of the sphere has been calculated on the basis of the data of Baker et al.[70] In the figure the dotted symbols (▼) are the recalculated effective radii of the latex sphere, and they fall exactly on the master curve. A master fit of the data gives a stretched exponential power of $\delta = 0.95$ and a prefactor $\beta = 2.2$. The δ value is close to the theoretical predicted value, 1, by Cukier[15] and Altenberger et al.[16] The fact that the stretched exponential power is close to 1 also indicates the diffusion in the polymer solution is a single relaxation process.

If the diffusion were through a mean field (the continuum Stokes approximation, eq 3), then $D\eta/D_0\eta_s$ should be universal and equal to 1.[20,27] To demonstrate that for the diffusion of the mesoscopic scale probes (where $2R/\xi \approx 1$) the continuum approximation fails, the viscosities of PEO (MW = 200 000) solutions were also measured. In Figure 13, $D\eta/D_0\eta_s$ is plotted as a function of polymer concentration for the diffusion of ovalbumin in PEO solutions. Positive deviations from eq 3 were observed over the concentration range studied. The probe diffuses faster than predicted by the Stokes−Einstein equation, since the probe does not "feel" the macroscopic viscosity of the solution.

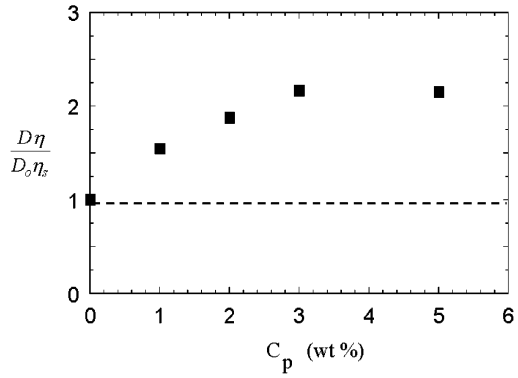

Figure 13. Product of the probe diffusivity and the solution viscosity normalized by the corresponding values at zero polymer concentrations as a function of PEO concentration. The dashed line represents the Stokes−Einstein equation (eq 3).

The scaling law serves as a good description for the diffusion of mesoscopic probes in the concentration ranges where the probe size is comparable to the polymer mesh size. However, for a given probe (R fixed), the reduced diffusion coefficient is expected to deviate from the master curve when polymer concentration c is not significantly above the overlap concentration c^*. The blank square in Figure 12 is the diffusion coefficient of G8 at $c = 0.5$ wt %, smaller than c^* (∼0.6). The diffusion coefficient becomes faster than that predicted by the master curve. This is reasonable because the matrix polymer is not a continuous network below c^*. At the other extreme, when $R/\xi \gg 1$, the reduced diffusion coefficient should be predicted by the Stokes−Einstein equation (eq 3), as the polymer solution becomes a continuum on the length scale of probe size R.

4. Conclusions

In this study, we have applied fluorescence recovery after photobleaching (FRAP) to follow the diffusion of mesoscopic probes (1 nm < R < 20 nm) in aqueous poly(ethylene oxide) (PEO) and guar galactomannan solutions. Two different FRAP techniques, fringe pattern bleaching and recovery (FPBR) and confocal scanning laser microscopy (CSLM), were used, and they were shown to yield consistent diffusion results. The framework for understanding the effects of the probe morphology and size and matrix polymer concentration and molecular weight is based on three criteria:

(1) R/ξ: The size of the diffusing probe, R, relative to the characteristic size of the polymer matrix mesh, ξ. This study focus on the mesoscopic regime where $R \cong \xi$.

(2) d_f: The fractal dimension of the diffusing species that determines the amount of interpenetration between the diffusing species and the matrix. This effect becomes increasingly important as R/ξ increases.

(3) τ_r/τ_d: The dynamics of constraint release in the polymer matrix τ_r relative to the dynamics of probe motion τ_d through a fluctuating matrix with constant topology.

The role of probe/matrix interpenetration was studied by comparing probes with different fractal dimensions d_f. Proteins and polystyrene latex particles can be treated as rigid spheres $d_f \sim 3$; dextrans are slightly branched polymers with a more expanded conformation ($d_f \sim 2.3$); dendrimers fall between these two with a density first decreasing and then increasing with generation. Dendrimers at low generations (G0) and high generations (G10) are similar to rigid spheres, while the intermediate generations (G2−G7) are more porous and expanded.

In addition, the diffusion of dextrans was shown to be less hindered in polymer solutions than rigid spheres when both have the same diffusion coefficients in free solution. The difference in diffusion coefficients is more pronounced at higher probe molecular weight. This is a result of the ability of the low fractal dimension, $d_f = 2.3$, dextrans to interpenetrate and deform as they pass through the matrix polymer mesh. The scaling equation $D/D_0 = \exp[-\beta(R/\xi)^\delta]$ was used to fit experimental results in the concentration ranges where the probe size is comparable to the polymer mesh size. A master curve for different probes was obtained, supporting a scaling theory model. For the compact probes ($d_f = 3$) the scaling coefficients are $\delta = 0.95$ and $\beta = 2.2$ for diffusion through PEO.

When the molecular weight of the matrix polymer is high enough, diffusion then becomes independent of matrix molecular weight (criterion 3) as demonstrated for PEO chains over a range of molecular weights at 10 wt % polymer. But when molecular weight of the matrix polymer is decreased at constant concentration or the concentration is decreased at constant (low) molecular weight, then faster dynamics due to constraint release are observed. The independence of diffusion coefficient from molecular weight verifies the assumptions of the classical scaling theories of diffusive motion.

The effect of matrix polymer stiffness was also addressed. Polymers with higher chain rigidities tend to have more hindrance on the probe diffusion than do flexible polymers, which is reflected in the prefactor β for flexible PEO with a persistence length of 8 Å and for guar with a persistence length of 40 Å. The effect of this extra length scale (persistence length) on the crossovers into the mesoscopic diffusion regime as a function of polymer concentration and molecular weight is largely unexplored and should provide fruitful directions for future experimental and theoretical studies. Direct measurements of chain dynamics using techniques such as NMR or spin-echo neutron scattering might provide further insight into the role of chain fluctuations on probe diffusion.

Acknowledgment. Support of this work by the National Science Foundation (NSFBES-9711781) is gratefully acknowledged.

References and Notes

(1) Jain, R. K. *Sci. Am.* **1994**, *271*, 58.
(2) Jain, R. K. *Nat. Med. (N.Y.)* **1998**, *4*, 655.
(3) Lebrun, L.; Junter, G. A. *Enzyme Microbial Technol.* **1993**, *15*, 1057.
(4) Moussaoui, M.; Benlyas, M.; Wahl, P. *J. Chromatogr.* **1992**, *591*, 115.
(5) Davidson, M. G.; Deen, W. M. *Macromolecules* **1988**, *21*, 3474.
(6) Tayal, A. In *Chemical Engineering*; North Carolina State University: Raleigh, NC, 1997.
(7) Cheng, Y.; Prud'homme, R. K. *Biomacromolecules* **2000**, *1*, 782.
(8) Doi, M.; Edwards, S. F. *The Theory of Polymer Dynamics*; Clarendon Press: Oxford, 1986.
(9) Graessley, W. W. *Adv. Polym. Sci.* **1982**, *47*, 67.
(10) Ianniruberto, G.; Marrucci, G. *J. Rheol.* **2001**, *45*, 1305.
(11) Pattamaprom, C.; Larson, R. G. *Rheol. Acta* **2001**, *40*, 516.
(12) Tasaki, H.; Takimoto, J.; Doi, M. *Comput. Phys. Commun.* **2001**, *142*, 136.
(13) de Gennes, P. G. *Scaling Concepts in Polymer Physics*; Cornell University Press: Ithaca, NY, 1979.
(14) Langevin, D.; Rondelez, F. *Polymer* **1978**, *19*, 875.
(15) Cukier, R. I. *Macromolecules* **1984**, *17*, 252.
(16) Altenberger, A. R.; Tirrell, M. *J. Chem. Phys.* **1984**, *80*, 2208.
(17) Phillies, G. D. J.; Ullmann, G. S.; Ullmann, K.; et al. *J. Chem. Phys.* **1985**, *82*, 5242.
(18) Phillies, G. D. J. *J. Phys. Chem.* **1989**, *93*, 5029.
(19) Streletzky, K. A.; Phillies, G. D. J. *J. Chem. Phys.* **1998**, *108*, 2975.
(20) Tong, P.; Ye, X.; Ackerson, B. J.; et al. *Phys. Rev. Lett.* **1997**, *79*, 2363.
(21) Ye, X.; Tong, P.; Fetters, L. J. *Macromolecules* **1998**, *31*, 5785.
(22) Masaro, L.; Zhu, X. X. *Prog. Polym. Sci.* **1999**, *24*, 731.
(23) Amsden, B. *Macromolecules* **1998**, *31*, 8382.
(24) Mustafa, M. B.; Tipton, D. L.; Barkley, M. D.; et al. *Macromolecules* **1993**, *26*, 370.
(25) Yang, T.; Jamieson, A. M. *J. Colloid Interface Sci.* **1988**, *126*, 220.
(26) Furukawa, R.; Arauzlara, J. L.; Ware, B. R. *Macromolecules* **1991**, *24*, 599.
(27) Won, J.; Onyenemezu, C.; Miller, W. G.; et al. *Macromolecules* **1994**, *27*, 7389.
(28) Lin, T. H.; Phillies, G. D. J. *J. Colloid Interface Sci.* **1984**, *100*, 82.
(29) Bu, Z.; Russo, P. S. *Macromolecules* **1994**, *27*, 1187.
(30) Prosa, T. J.; Bauer, B. J.; Amis, E. J.; et al. *J. Polym. Sci., Part B: Polym. Phys.* **1997**, *35*, 2913.
(31) Yu, K.; Russo, P. S. *J. Polym. Sci., Part B: Polym. Phys.* **1996**, *34*, 1467.
(32) Muhr, A. H.; Blanshard, J. M. V. *Polymer* **1982**, *23*, 1012.
(33) Westrin, B. A.; Axelsson, A.; Zacchi, G. *J. Controlled Release* **1994**, *30*, 189.
(34) Huang, W. J.; Frick, T. S.; Landry, M. R.; et al. *AIChE J.* **1987**, *33*, 573.
(35) Lodge, T.; Chapman, B. *Trends Polym. Sci.* **1997**, *5*, 122.
(36) Gribbon, P.; Hardingham, T. E. *Biophys. J.* **1998**, *75*, 1032.
(37) Gribbon, P.; Heng, B. C.; Hardingham, T. E. *Biophys. J.* **1999**, *77*, 2210.
(38) Pluen, A.; Netti, P. A.; Jain, R. K.; et al. *Biophys. J.* **1999**, *77*, 542.
(39) Meyvis, T. K. L.; De Smedt, S. C.; Van Oostveldt, P.; et al. *Pharm. Res.* **1999**, *16*, 1153.
(40) Tseng, K. C.; Turro, N. J.; Durning, C. J. *Polymer* **2000**, *41*, 4751.
(41) Fox, J. E. In *Thickening and Gelling Agents for Food*; Imeson, A., Ed.; Blackie Academic Professional: New York, 1997; p 262.
(42) Prudhomme, R. K.; Constien, V.; Knoll, S. *Adv. Chem. Ser.* **1989**, 89.
(43) Brode, G. L.; Goddard, E. D.; Harris, W. C.; et al. In *Cosmetic and Pharmaceutical Applications of Polymers*; Gebelein, C. G., Cheng, T. C., Yang, V. C., Eds.; Plenum: New York, 1991; p 117.
(44) Tseng, K. C.; Turro, N. J.; Durning, C. J. *Phys. Rev. E* **2000**, *61*, 1800.
(45) Tseng, K. C. Department of Chemical Engineering and Applied Chemistry, Columbia University, New York, 1998.
(46) Crank, J. *The Mathematics of Diffusion*; Clarendon Press: Oxford, 1979.
(47) Chaikin, P. M.; Lubensky, T. C. *Principles of Condensed Matter Physics*; Cambridge University Press: Cambridge, 1995.
(48) Tanford, C. *Physical Chemistry of Macromolecules*; John Wiley & Sons: New York, 1961.
(49) Smit, J. A. M.; Vandijk, J.; Mennen, M. G.; et al. *Macromolecules* **1992**, *25*, 3585.
(50) Zallen, R. *The Physics of Amorphous Solids*; John Wiley & Sons: New York, 1998.
(51) Meltzer, A. D.; Tirrell, D. A.; Jones, A. A.; et al. *Macromolecules* **1992**, *25*, 4549.
(52) Meltzer, A. D.; Tirrell, D. A.; Jones, A. A.; et al. *Macromolecules* **1992**, *25*, 4541.
(53) Gaube, J.; Pfennig, A.; Stumpf, M. *Fluid Phase Equilib.* **1993**, *83*, 365.

(54) Gaube, J.; Pfennig, A.; Stumpf, M. *J. Chem. Eng. Data* **1993**, *38*, 163.
(55) King, R. S.; Blanch, H. W.; Prausnitz, J. M. *AIChE J.* **1988**, *34*, 1585.
(56) Ogston, A. G.; Preston, B. N.; Wells, J. D. *Proc. R. Soc. London, Ser. A* **1973**, *333*, 297.
(57) Vrentas, J. S.; Duda, J. L. *AIChE J.* **1979**, *25*, 1.
(58) Brandrup, J.; Immergut, E. H. John Wiley & Sons: New York, 1975.
(59) Kawaguchi, S.; Imai, G.; Suzuki, J.; et al. *Polymer* **1997**, *38*, 2885.
(60) Marchessault, R. H.; Buleon, A.; Deslandes, Y.; et al. *J. Colloid Interface Sci.* **1979**, *71*, 375.
(61) Petkowicz, C. L. O.; Milas, M.; Mazeau, K.; et al. *Food Hydrocolloids* **1999**, *13*, 263.
(62) Robinson, G.; Ross-Murphy, S. B.; Morris, E. R. *Carbohydr. Res.* **1982**, *107*, 17.
(63) Bailey, F.; Kucera, J. L.; Imhof, L. G. *J. Polym. Sci.* **1958**, *32*, 517.
(64) Stuart, M. A. C.; Waajen, F.; Cosgrove, T.; et al. *Macromolecules* **1984**, *17*, 1825.
(65) Polverari, M.; vandeVen, T. G. M. *J. Phys. Chem.* **1996**, *100*, 13687.
(66) Baumgaertel, M.; Schausberger, A.; Winter, H. H. *Rheol. Acta* **1990**, *29*, 400.
(67) Graessley, W. W. *Adv. Polym. Sci.* **1974**, *16*, 1.
(68) Wu, S. H. *J. Polym. Sci., Part B: Polym. Phys.* **1987**, *25*, 2511.
(69) Gittings, M. R. Ph.D. Thesis, Department of Chemical Engineering, Princeton University, 1998.
(70) Baker, J. A.; Pearson, R. A.; Berg, J. C. *Langmuir* **1989**, *5*, 339.

MA0107758